Asian Journal of Chemistry; Vol. 32, No. 8 (2020), 2013-2020

ASIAN JOURNAL OF CHEMISTRY

https://doi.org/10.14233/ajchem.2020.22725

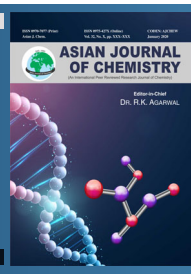

# Lanthanum Doped Strontium Titanate Nanomaterial for Photocatalytic and Supercapacitor Applications

V.V. DESHMUKH[1,*], H.P. NAGASWARUPA[2], C.R. RAVIKUMAR[3,*], M.R. ANIL KUMAR[3], T.R. SHASHI SHEKHAR[3] and H.C. ANANDA MURTHY[4]

[1]Department of Physics, Shri Shivaji Science College, Amravati-444602, India
[2]P.G. Department of Chemistry, Davanagere University, Davanagere-577001, India
[3]Research Centre, Department of Science, East West Institute of Technology, Bangalore-560091, India
[4]Department of Applied Chemistry, School of Applied Natural Science, Adama Science and Technology University, PO Box 1888, Adama, Ethiopia

*Corresponding authors: vaishalideshmukh27@gmail.com; ravicr128@gmail.com

*Received*: 16 March 2020; *Accepted*: 21 May 2020; *Published online*: 27 July 2020; AJC-19983

We report the synthesis of lanthanum doped strontium titanate ($Sr_{1-x}La_xTiO_3$,x=0.1) by sol-gel method. The physical properties of the as-synthesized sample were systematically studied through X-ray powder diffraction (XRD), scanning electron microscopy (SEM), transmission electron microscopy (TEM) and energy dispersive X-ray spectroscopy (EDAX). Diffraction peaks in XRD supported the cubic formation of perovskite-type crystal structure. The image analysis of nanomaterial by SEM and TEM techniques disclosed aggregates of nanoparticles with grain size about 20 nm. The study by UV-DRS exposed the band energy gaps ($E_g$) of 3.4 eV for strontium titanate nanoparticles, respectively. The degradation studies for three days were carried out for three dyes. Malachite green and rhodamine blue, strontium titanate nanoparticles showed utmost photocatalytic activity for rhodamine blue under UV light irradiation (from 0 to 80 min) as compared to malachite green. Properties of electrochemistry were looked into by cyclic voltammetry and galvanostatic charge/discharge in 1M KCl electrolyte. The $Sr_{0.9}La_{0.1}TiO_3$ electrode displayed maximal specific capacitance of 306.74 F $g^{-1}$ at current 1mA from galvanostatic charge-discharge curve. The rare earth doped perovskite $Sr_{0.9}La_{0.1}TiO_3$ nanomaterial exhibited increased surface area with superior supercapacitance property.

**Keywords: Supercapacitor, $Sr_{0.9}La_{0.1}TiO_3$, Perovskite, Cyclic voltammetry, Capacitive performance.**

## INTRODUCTION

The present world is in need of modern, smart and energy efficient materials. Significant amount of work has been happening in this regard to explore broad range of options for energy harvesting, storage and conversion. The supercapacitors have recently gained wide popularity due to quite range of possibilities such as high power density, long cycle life and it links the power/energy gap between traditional dielectric capacitors and batteries/fuel cells [1-4]. Transition metal oxides gain notable attention in the area of energy storage/conversion not just due to their superior mechanical, structural, or electronic properties but also because of their high pseudo capacitances which is possibly believed to be due to their multiple valence state changes, generally not expected in case of carbon materials [5-7]. Oxides with perovskite structure have recently proven as the best option due to their high specific capacitance and large operating window [8-9] over the large choices of transition metal oxides that are verified as super capacitor. Doped strontium titanate, a ceramic material with $ABO_3$ perovskite structure, found to exhibit superconductivity [10]. The conduction can be achieved by n-type doping making use of lanthanum (La). The substitution of $La^{3+}$ for $Sr^{2+}$ renders $SrTiO_3$ highly conductive [11,12]. The electronic properties of La doped $SrTiO_3$ attract notable attention due to its many potential applications [13]. Recently, it has been reported that lanthanum has obvious influence on the capabilities of many materials [14,15].

Numerous investigators had extended the preparation of La/N co-doped $SrTiO_3$ catalysts. Miyauchi *et al*. [16] accounted that the synthesis of $SrTiO_3$ catalysts with La/N co-doped by

sol-gel method reduced the vacancy of ions and then photocatalytic activity is raised in a visible light. Wang *et al*. [17] established that the synthesis of La/N co-doped $SrTiO_3$ catalysts using mechanochemical reaction improved the photocatalytic activity in a visible light. On the other hand, they had a particle of large size and small specific surface area which restricted the catalytic capability. To get better the photocatalytic ability, synthesis of very well particle which has a large specific surface area should be realize.

Sol-gel process provides various efficient advantages over traditional synthetic methods. It gives way to homogeneous mixing of reactants on the molecular level and can be adopted to control shape, morphology and particle size of the resulting product. In this work, we have synthesized La doped $SrTiO_3$ ($Sr_{0.9}La_{0.1}TiO_3$) by sol-gel method and investigated the electrochemical capacitor performances of as-synthesised material by making it as working electrode. The specific capacitance [18] and supercapacitance [19] of La doped $SrTiO_3$ has been tested. The microstructure, morphology and elemental analysis of the as prepared sample was systematically studied through X-ray powder diffraction (XRD), scanning electron microscopic (SEM), transmission electron microscopic (TEM) energy dispersive X-ray spectroscopic (EDAX), diffuse reflectance spectra (DRS), cyclic voltammetry (CV), electrochemical impedance spectra (EIS) and galvanostatic charge-discharge (GCD) techniques.

## EXPERIMENTAL

**Preparation of $Sr_{0.9}La_{0.1}TiO_3$ nanomaterial using sol-gel method:** Strontium nitrate ($Sr(NO_3)_2$) and lanthanum nitrate ($La(NO_3)_3$) salts were first dissolved in small amount of alcohol and then the mixture was poured into a solution of titanium tetra butoxide ($Ti(OC_4H_9)_4$). Citric acid was successively added to attain the molar ratio 2:1. This mixture was heated to about 80 ºC and stirred on magnetic stirrer for 3 h to obtain a gel. The gel is then transferred into an autoclave and heated to 130 ºC for 12 h. The resulting precipitate was calcined at two different conditions, one at 350 ºC for 3.5 h and the other at 550 ºC for 6 h.

**Characterizations:** The synthesized $Sr_{0.9}La_{0.1}TiO_3$ nanomaterial was characterized for its structural features by analytical X-ray diffractometer (X′pert pro MPD) equipped with Cu*K*α sealed tube (λ = 1.5406 Å). The sample was scanned over 2θ ranging from 20º to 80º with a step size of 0.016º. Morphology of the sample was examined by a Zeiss ultra plus FESEM instrument (tungsten filament is used in accelerating voltages upto 20 kV). Transmission electron microscopic (TEM) analysis was performed using PHILIPS, CM-200 machine (accelerating voltage up to 200 kV, 2.4 Å resolutions). Energy dispersive X-ray spectroscope (EDS) coupled to FESEM was used to analyze the composition of sample. Reflectance study was conducted by UV-vis spectrophotometer (UV 2600 double beam, Shimadzu). The cyclic voltammetric measurements were executed on an electrochemical analyzer CHI604E potentiostat with a tri-electrode system. The charge-discharge experiment was performed using a CHI600-2C work station. Impedance analysis was carried out at an open circuit potential (OCP) and data recorded over a frequency range of 0.1 Hz to 1 MHz with an AC voltage of amplitude 5 mV.

**Electrode preparation and electrochemical characterization:** A mixture of 80 wt% of $Sr_{0.9}La_{0.1}TiO_3$ nanomaterial and 20 wt% of binder polyvinylidene difluoride (PVDF) in *N*-methyl-2-pyrrolidone (NMP) was used to make working electrode. This uniform mixture was spread on gold plate with 1 mg/cm$^2$ and dried at room temperature overnight.

For cyclic voltammetric tests, the measurement was performed on an electrochemical analyser CHI604E potentiostat with a tri-electrode system, consisting of working ($Sr_{0.9}La_{0.1}TiO_3$) electrode with platinum wire and Ag/AgCl electrodes as counter and reference electrodes respectively and the electrolyte being a 1 M KCl solution. The potential range was held between -0.3 V to 0.3 V (*vs*. Ag/AgCl electrode) and the scanning rates were set to 1 mV/s, 3 mV/s and 5 mV/s during the experimentation. In addition, EIS measurements were also executed using AC amplitude of 5 mV with frequency ranging between 0.1 Hz and 1 MHz. The charge-discharge experiments were also carried out along with EIS measurements. All the above tests were performed at room temperature.

The specific capacitance (C, F g$^{-1}$) of the electrode calculated from the cyclic voltammetric curve and by using the equation is as given below:

$$C = \frac{1}{m.S.(V_a - V_c)} \int_{V_a}^{V_c} I_{(V)} dV \quad (1)$$

where m(g) is the mass of electroactive material loaded on the electrode, $V_a$, $V_c$ are the anodic and cathodic peak voltages, s (V s$^{-1}$) is the scan rate for the measurement and $\int I_{(V)}\ dV$ is the area under the cyclic voltammogram from $V_a$ to $V_c$.

The specific capacitance (C, F g$^{-1}$) of the electrode calculated from the galvanostatic charge-discharge (GCD) curve [5] as according to eqn. 2:

$$C = \frac{i}{-\frac{\Delta V}{\Delta t} \times m} = \frac{i}{-Slope \times m} \quad (2)$$

where i is the current applied, $\Delta V/\Delta t$ is the slope of the discharge curve after IR drop and m is the mass of active material on one electrode.

## RESULTS AND DISCUSSION

**Crystalline structure of $Sr_{0.9}La_{0.1}TiO_3$:** Fig. 1 shows the XRD pattern of $Sr_{0.9}La_{0.1}TiO_3$ nanomaterial at room temperature. The formation of $Sr_{0.9}La_{0.1}TiO_3$ perovskite crystals with same structure as pure $SrTiO_3$ was confirmed from the XRD result. The major peaks appeared for the nanomaterial corresponds to the crystal planes (100) (110) (111) (200) (211) (220) and (310).The XRD pattern shows that the sample contained minor impurity peaks and match with JCPDS card no. 00-035-0795. The pattern shows the clear single cubic phase without any secondary phase. The crystallite size was calculated by using Debye-Scherrer′s formula [20].

$$D = \frac{K\lambda}{\beta \cos\theta} \quad (3)$$

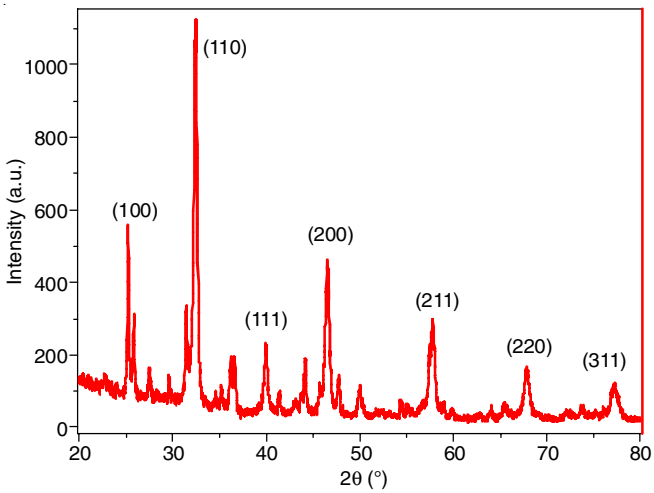


Fig. 1. XRD pattern of $Sr_{0.9}La_{0.1}TiO_3$ nanomaterial

An average crystallite sizes was found to be 22.2 nm for the peak at 2θ = 32.33º corresponding to (110) crystal plane and lattice parameter calculated as 3.9126 Å (a=b=c) for the same plane, which is in agreement with the other studies [21].

**Surface morphological analysis:** The supercapacitor application depends on the morphology of the material. The SEM images (Fig. 2) of $Sr_{0.9}La_{0.1}TiO_3$ nanomaterial exhibit porous and agglomerated structures. Electrode material indicating the irregularities in shapes and structures have a very few sugar-like shape with narrow size distribution.The chemical composition of $Sr_{0.9}La_{0.1}TiO_3$ nanomaterial is revealed by EDX studies (Fig. 3) which confirmed that the observed compositions were in accordance to the loaded ones. TEM images of $Sr_{0.9}La_{0.1}TiO_3$ are as shown in Fig. 4a. TEM showed the formation of nanoparticles of cubical shape with size ranging between 50 and 20nm. This result is in good agreement with the average particle size given by XRD characterization. Selected area electron

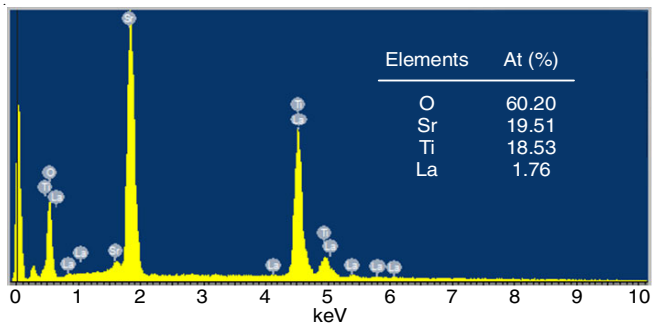


Fig. 3. EDX spectra showing the presence of $Sr_{0.9}La_{0.1}TiO_3$

diffraction spots can be observed in Fig. 4(b). Electron diffraction studies indicated crystalline nature of the sample [22].

**DRS analysis:** Fig. 5. shows the UV-Vis diffused reflectance spectra of $Sr_{0.9}La_{0.1}TiO_3$ nanomaterials. As shown form the spectra $Sr_{0.9}La_{0.1}TiO_3$ show a strong light absorbance edge close to 410 nm due to its inherent band gap (~3.4 eV) shown in inset Fig. 5. This displays considerable advancement of visible light reflection, therefore there is betterment in electrochemical reactions by visible light besides ultra-violet. Owing to unique half-filed electronic configuration of La, has the capacity to form new intermediate energy levels inside the band gap of $Sr_{0.9}La_{0.1}TiO_3$ and contracts the distance across the valence band and conduction band. The additional state leads to effective red-shift (longer wavelength) of the absorption threshold. The Kubelka-Munk function F(R) is for the most part connected to change over the diffused reflectance into equivalent absorption coefficient and utilized for examining the powders [23] as given by eqn. 4:

$$F(R) = \frac{(1-R)^2}{2R} \quad (4)$$

where R: the reflectance, F(R): Kubelka-Munk function. The optical energy gap was calculated using Tauc relation; the band

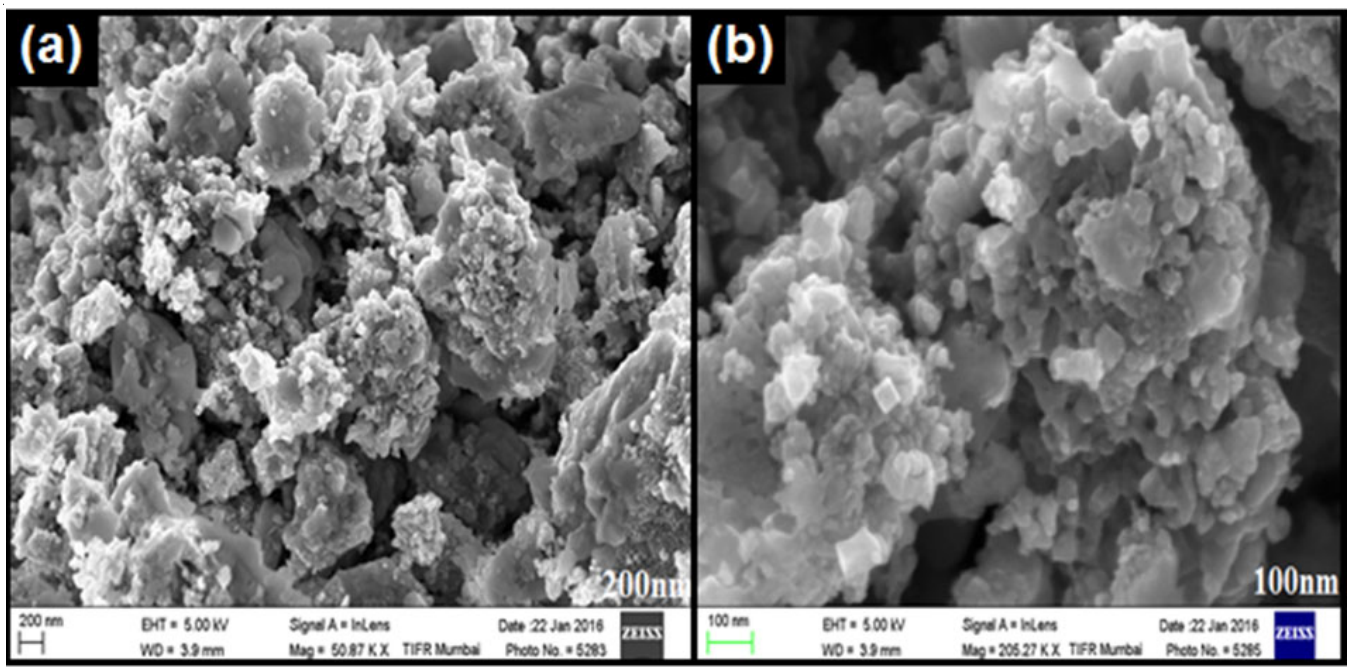


Fig. 2. FE-SEM images of $Sr_{0.9}La_{0.1}TiO_3$ at magnification (a) 50.87 KX (b) 205.27 KX

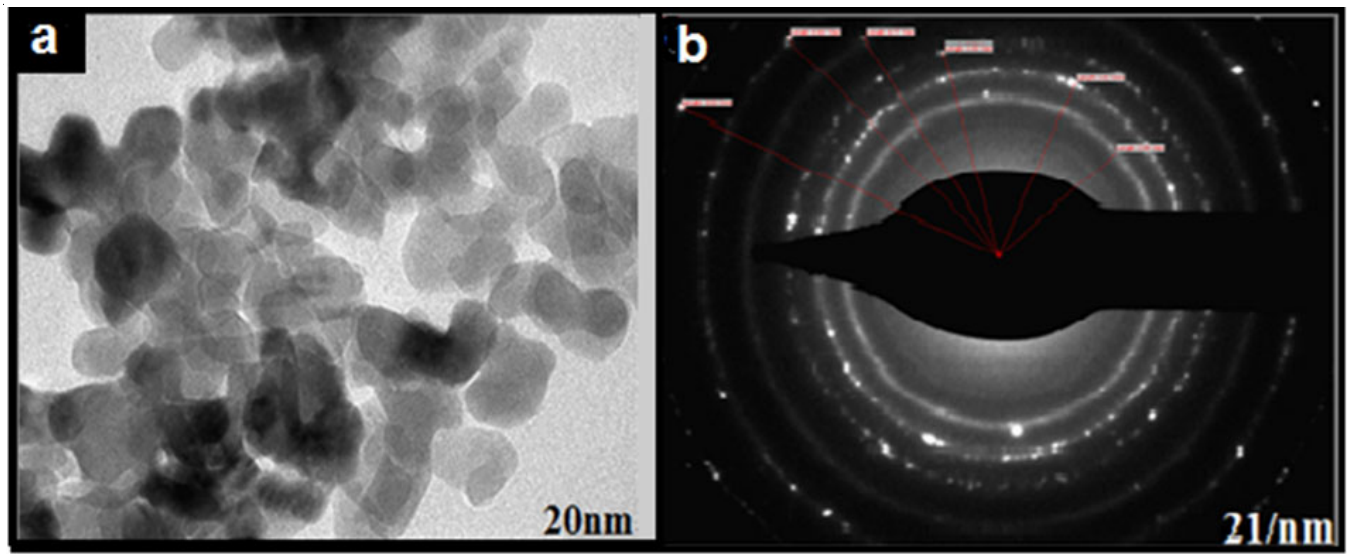


Fig. 4. (a) TEM images of $Sr_{0.9}La_{0.1}TiO_3$, (b) In the inset, electron diffraction spots are observed

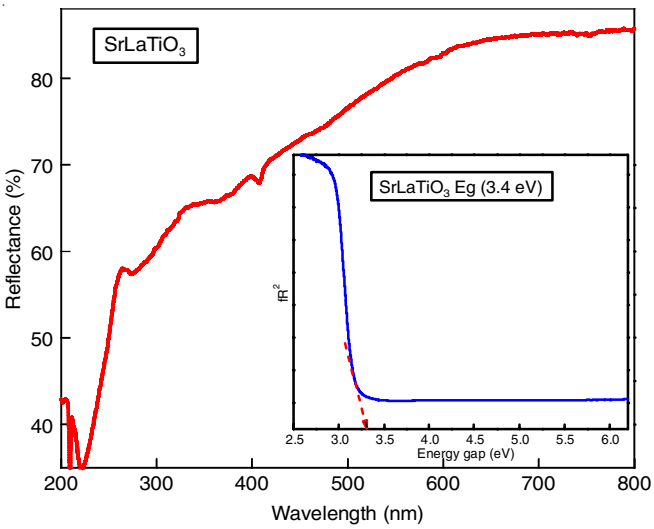


Fig. 5. DRS and energy gap graphs of $Sr_{0.9}La_{0.1}TiO_3$ nanomaterials

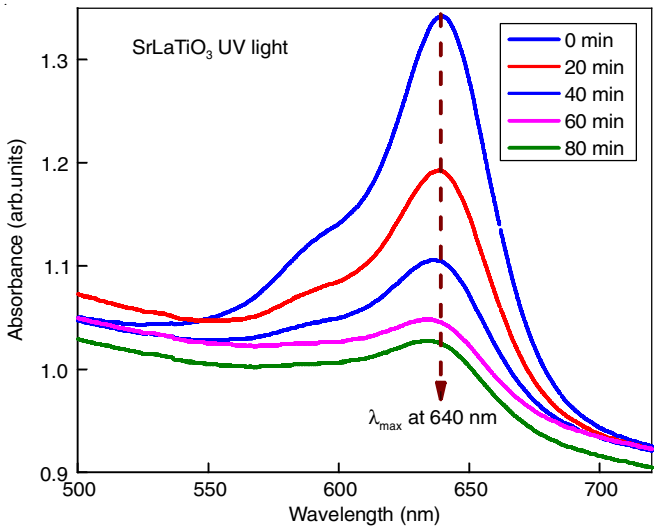


Fig. 6. Absorbance spectra of malachite green for $Sr_{0.9}La_{0.1}TiO_3$ nanomaterials under UV light irradiation

gap ($E_g$) of semiconductor material can be calculated from eqn. 5:

$$F(R)\ h\nu = A\ (h\nu - Eg)^n \quad (5)$$

where n = 1/2 and 2 for direct and indirect transitions respectively, it giving the indirect band and direct band. Tauc relation was used to calculate optical energy gap as in eqn. 5 thereby given the direct band [24].

**Photocatalytic activity of dyes:** Malachite green and rhodamine-B photo-decolarization by using $Sr_{0.9}La_{0.1}TiO_3$ nanomaterials as a photo-catalyst of UV-Vis absorption spectral changes under UV light irradiation are shown in Figs. 6 and 7. It is valuable to highlight that $Sr_{0.9}La_{0.1}TiO_3$ nanomaterials sample shown the better photo-catalytic activity under UV light irradiation for rhodamine-B dye compared to malachite green. The UV-visible absorption spectra alterations of photocatalytic degradation for rhodamine-B and malachite green under simulated UV light irradiation is looking that the maximum absorption band reduced slowly on the wavelength of 484 and

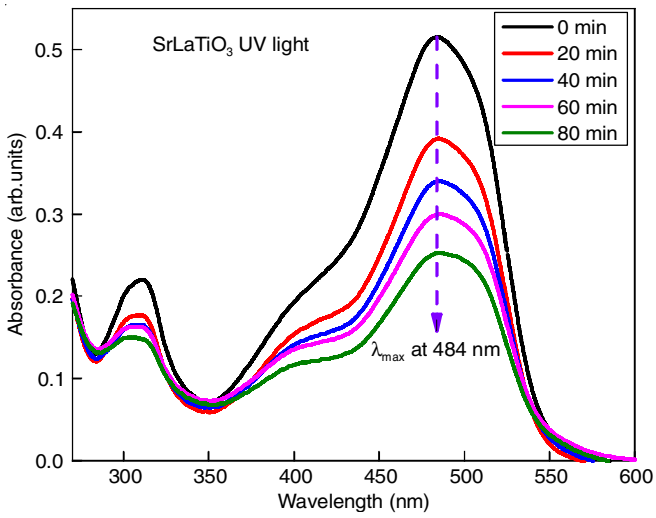


Fig. 7. Absorbance spectra of Rh-B for $Sr_{0.9}La_{0.1}TiO_3$ nanomaterials under UV light irradiation

640 nm due to greater irradiation time then rhodamine-B and malachite green is being degradation progressively. In addition, the maximal absorption band of rhodamine-B has no notable change. This might be conditional that rhodamine-B and malachite green commonly suffers a comparatively too easy cleavage of the whole conjugated chromophore. The maximum absorption band refuses penetratingly, which shows that rhodamine-B molecules are almost decaying completely.

Above the outcome may depend on fuel used during the synthesis and due to the dye sensitization, may be attributed to small crystallite size, narrow energy gap, textural properties and potential for reducing the $e^{-}$-$h^{+}$ pair recombination used to be found making use of special photocatalyst. It was evident that the development fee of hydroxyl ions on the MNP used to be advanced than that of different products, which used to be also regular with the outcome of energy gap of the substances, Additionally, suggesting that MNP was once an excellent path to accelerate the interfacial charge transfer and reduce the recombination of $e^{-}$-$h^{+}$ pairs, which resulted with increase in hydroxyl ions formation [25].

## Electrochemical analysis

**Cyclic voltammetry:** The cyclic voltammetric response of $Sr_{0.9}La_{0.1}TiO_3$ electrode at different scan rates of 1 mV/s, 3 mV/s and 5 mV/s are presented in Fig. 8a. The cyclic voltammograms were cycled between -0.3 V and 0.3 V. The cyclic voltammograms started at -0.3 V reversed at 0.3 V and terminated at -0.3V. Here, capacitance was mainly based on redox reaction because the shape of cyclic voltammograms as distinguished from the shape of electric double layer capacitance, which is usually similar to rectangle [26-30]. As it can be seen during cyclic voltammograms scan, two well-defined peaks were appeared.

The difference in potential is due to reversible electrode reaction, $E_O - E_R$; smaller the difference, greater is the reversibility [5]. Fig. 8a makes it clear that calculated $E_O - E_R$ value was to be 0.627 V at 1 mV/s scan rate, it shows the charge efficiency and the electrode reversibility was found to be superior [25].

The anodic peak being centred at around (0.052 V) and cathodic peak centred at around (-0.014 V) for the scan rate of

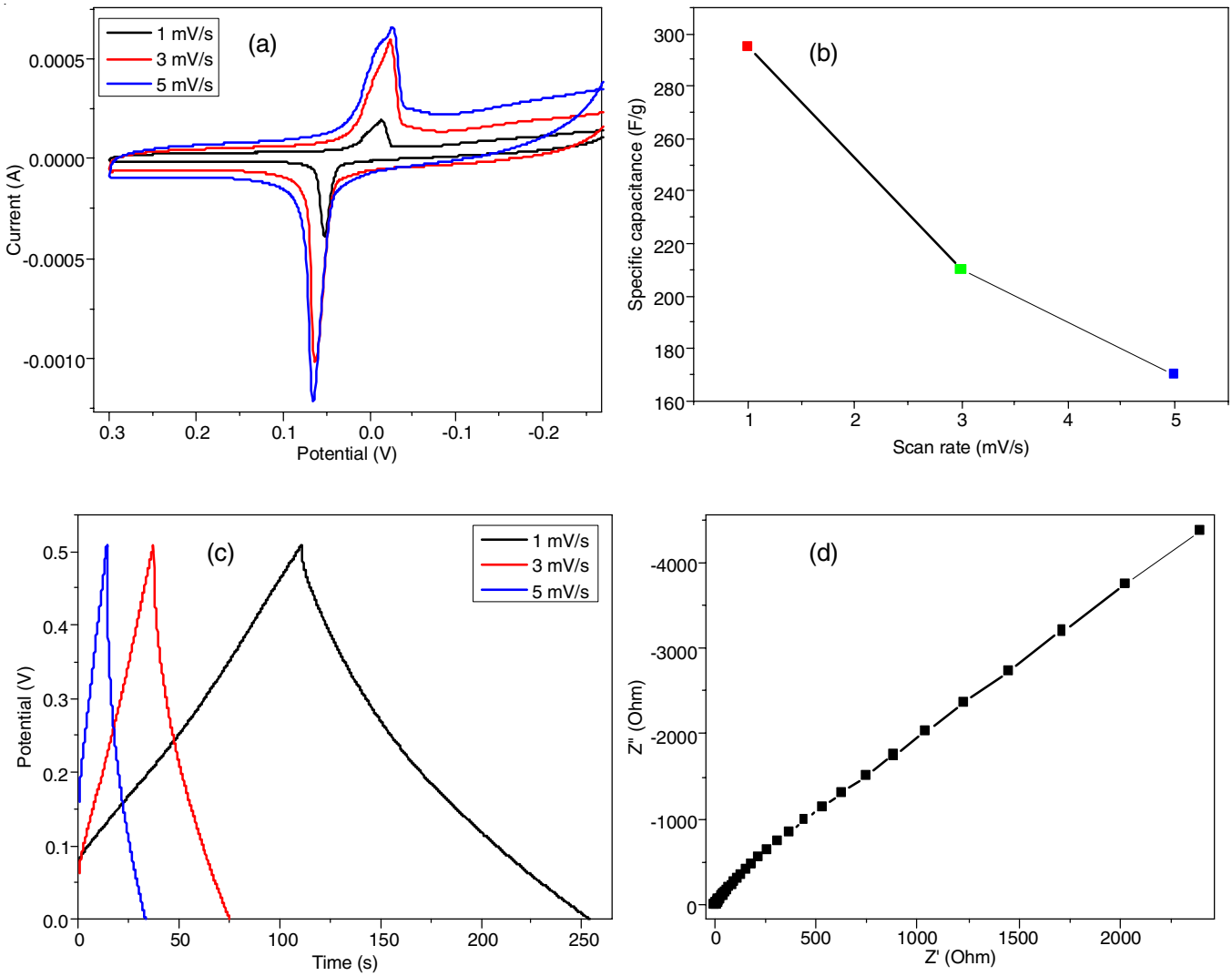


Fig. 8. (a) Cyclic voltammogram at scan rate 1, 3 and 5 mV/s (b) Scan rate *vs.* specific capacitance (c) Galvanostatic charge-discharge curve at different scan rates (d) EIS spectra of nanostructured $Sr_{0.9}La_{0.1}TiO_3$ electrode in 1 M KCl

1 mV/s. These two peaks indicate the reversible redox process in the aqueous solution which represents the Faradic pseudo-capacitive behaviour. The specific capacitance calculated from the cyclic voltammograms using eqn 1. Maximum capacitance of 297.89 F $g^{-1}$ was obtained at the scan rate of 1 mV/s. It indicates good performance of nanostructured $Sr_{0.9}La_{0.1}TiO_3$ electrode [31]. The specific capacitance of the nanostructured electrode decrease with the increase of scan rate (Table-1). This is because of the fact that higher scan rate limits the accessibility of ions inside every pore of the electrode and only the outermost portion of the electrode is utilized for the ion diffusion. However, specific capacitance is 170.89 F at higher scan rate of 5 mV/s.

TABLE-1
SPECIFIC CAPACITANCE OF $Sr_{0.9}La_{0.1}TiO_3$ SAMPLE CALCULATED FROM CV AND GCD AT DIFFERENT SCAN RATE AND DISCHARGE CURRENT DENSITY

| Specific capacitance calculated from CV | | Specific capacitance calculated from GCD | |
|---|---|---|---|
| Scan rate (mV/s) | Specific capacitance (F/g) | Discharge current (mA) | Specific capacitance (F/g) |
| 1 | 297.89 | 1 | 306.74 |
| 3 | 206.88 | 3 | 265.95 |
| 5 | 170.89 | 5 | 252.14 |

**Galvanostatic charge-discharge (GCD):** The electrochemical characteristics of $Sr_{0.9}La_{0.1}TiO_3$ electrode were also evaluated by galvanostatic charge-discharge measurement. The charge/discharge curves of $Sr_{0.9}La_{0.1}TiO_3$ at different current densities of 1, 2 and 3 mA/$cm^2$ in 1M KOH are shown in Fig. 8c. Symmetric charge-discharge features were displayed, indicating good pseudo-capacitive behaviours and excellent reversible redox reaction characteristics [32,33]. It is observed that the charging curves are quite mirror symmetric to their discharge counterparts in the whole potential range because of the redox reaction occurring on the surface of $Sr_{0.9}La_{0.1}TiO_3$ electrode. The $Sr_{0.9}La_{0.1}TiO_3$ presents the longest charging time and the highest capacitance, which is in good agreement with the CV results. The maximum discharge specific capacitance of $Sr_{0.9}La_{0.1}TiO_3$ samples calculated from the GCD curve using eqn 2 at current 1 mA is 306.74 F $g^{-1}$. The specific capacitance decreases with the increase in discharge current (Fig. 8b and

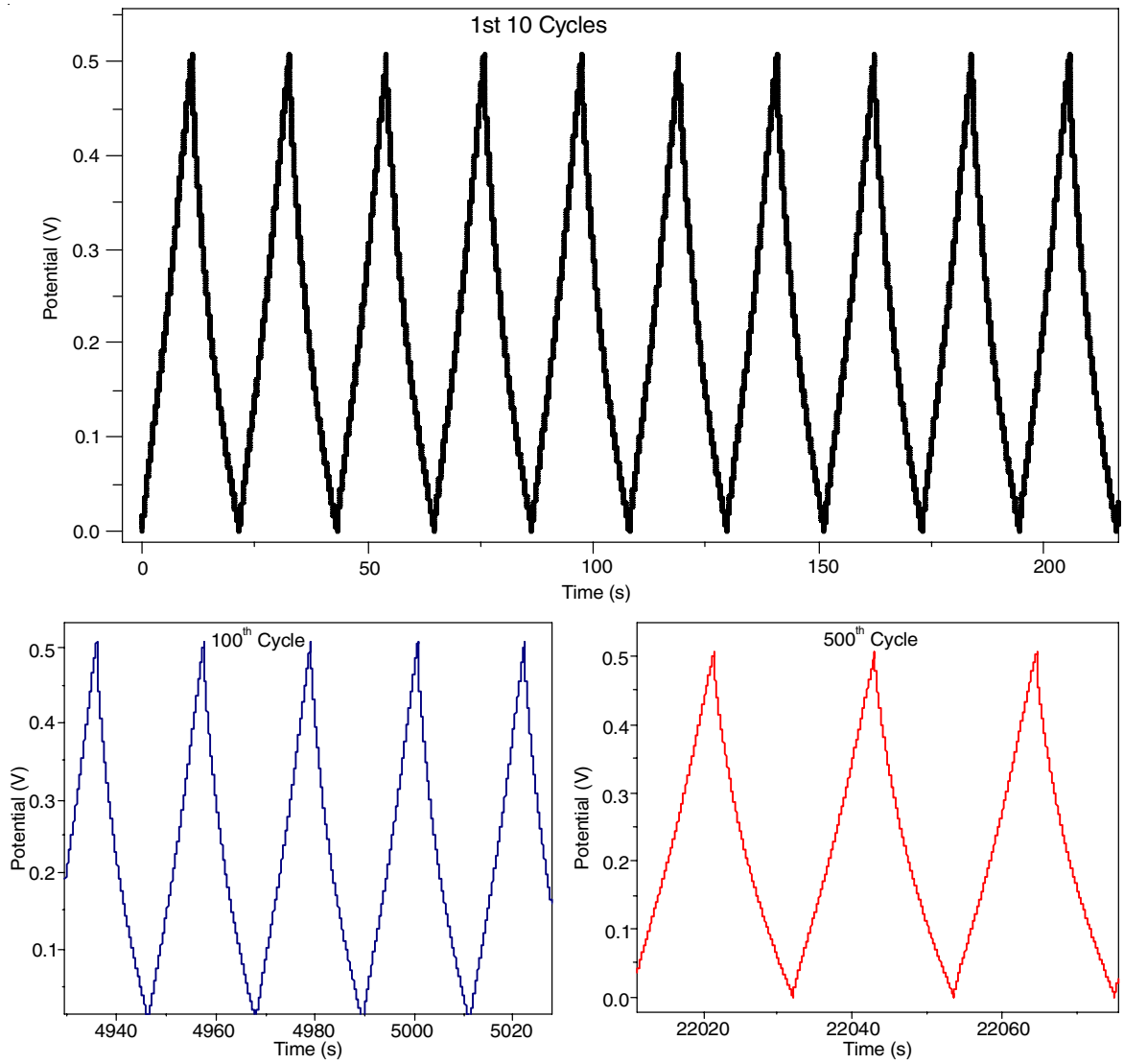


Fig. 9. Galvanostatic charge-discharge curve of $Sr_{0.9}La_{0.1}TiO_3$ electrode for different cycles at 5 mV/s scan rate

Table-1). It is perhaps accepted that during the Faradic redox reaction, when the density current is smaller, the ion and the electron may have more time to diffuse through the interface/ surface of the porous electrode.

**Electrochemical impedance spectroscopy (EIS):** Fig. 8d shows Nyquist plot of $Sr_{0.9}La_{0.1}TiO_3$ electrode The Nyquist plot had high frequency region comprised in a small semi circle accompanied by a straight line in the low frequency region. The absence of distinct semi-circle in the plots shows slight charge transfer resistance at the modified electrode/ electrolyte interface. The imaginary part of the impedance spectra at low frequencies represents the capacitive nature of the electrode and approaches a straight line in an ideal capacitor [34].

The life cycle stability of $Sr_{0.9}La_{0.1}TiO_3$ electrode was performed using galvanostatic charge-discharge curves (Fig. 9) measured at a current density of 5 A $g^{-1}$ for 500 cycles within the potential window of 0 to 0.5 V *vs*. Ag/AgCl. $Sr_{0.9}La_{0.1}TiO_3$ electrode showed very good cycling stability. Thus the electrode could maintain more than 95% of its original capacitance in 1 M KOH even after 500 cycles.

## Conclusion

A $Sr_{0.9}La_{0.1}TiO_3$ nanomaterial was successfully prepared by using sol-gel method. According to XRD results $Sr_{0.9}La_{0.1}TiO_3$ exhibits cubic perovskite $ABO_3$ type crystal structure nanocomposite with an average crystalline domain of 20 nm. Microstructure through SEM revealed sugar crystal like nature of the material. The energy band gap was found to be 3.4 for $Sr_{0.9}La_{0.1}TiO_3$ nanoparticles, the PCA studied for malachite green and rhodamine-B, the synthesized $Sr_{0.9}La_{0.1}TiO_3$ nanoparticles showed highest PCA for rhodamine-B under UV light irradiation (from 0 to 80 min). Electrochemical properties of sample were investigated in detail by cyclic voltammetry and galvanostatic charge-discharge. A $Sr_{0.9}La_{0.1}TiO_3$ electrode shows maximum specific capacitance of 306.74 F $g^{-1}$ at current density 1 mA/$cm^2$ from GCD curve. It was demonstrated that La doping resulted in significant improvements in specific capacitance. Moreover, it is an effective method to overcome the intrinsic low conductivity of $SrTiO_3$. Appropriate amount of doped La can increase the surface area of synthesized material, resulting in the super capacitive behaviour enhancement. This nanomaterial also exhibited better cyclic capability rate of charge-discharge.

## ACKNOWLEDGEMENTS

The authors are grateful to Nanotechnology Research lab, Department of Chemistry, Shri Shivaji Science College, Amravati, India for providing research facilities. Two of the authors, MRA and CRR thank VGST, Government of Karnataka, India (No: VGST/CISEE/2014-15/282) and (VGST/K-FISTL1/ 2014-15/ GRD-360) for extending their support to carry out this research work.

## CONFLICT OF INTEREST

The authors declare that there is no conflict of interests regarding the publication of this article.

## REFERENCES

1. B.E. Conway, Electrochemical Supercapacitors: Scientific Fundamentals and Technological Applications, Springer Science+Business Media: New York (1999).
2. C.R. Ravikumar, P. Kotteeswaran, V.B. Raju, A. Murugan, M.S. Santosh, H.P. Nagaswarupa, S.C. Prashantha, M.R.A. Kumar and M.S. Shivakumar, *J. Energy Storage*, **9**, 12 (2017); https://doi.org/10.1016/j.est.2016.11.001
3. C.R. Ravikumar, P. Kotteeswaran, A. Murugan, V. Bheema Raju, M.S. Santosh, H.P. Nagaswarupa, H. Nagabhushana, S.C. Prashantha, M.R. Anil Kumar and K. Gurushantha, *Mater. Today Proc.*, **4**, 12205 (2017); https://doi.org/10.1016/j.matpr.2017.09.151
4. K.M. Ajay, M.N. Dinesh, K.A. Vishnu Murthy, C.R. Ravikumar and H.P. Nagaswarupa, *Mater. Today: Proceed.*, **5**, 21452 (2018); https://doi.org/10.1016/j.matpr.2018.06.554
5. C.R. Ravikumar, M.R.A. Kumar, H.P. Nagaswarupa, S.C. Prashantha, A.S. Bhatt, M.S. Santosh and D. Kuznetsov, *J. Alloys Compd.*, **736**, 332 (2018); https://doi.org/10.1016/j.jallcom.2017.11.111
6. C. Yi, J. Zou, H. Yang and X. Leng, *Trans. Nonferrous Met. Soc. China*, **28**, 1980 (2018); https://doi.org/10.1016/S1003-6326(18)64843-5
7. T. Brezesinski, J. Wang, S. Tolbert and B. Dunn, *J. Sol-Gel Sci. Technol.*, **57**, 330 (2011); https://doi.org/10.1007/s10971-010-2183-z
8. N. Arjun, G. Pan and C.K. Yang, *Results in Physics*, **7**, 920 (2017); https://doi.org/10.1016/j.rinp.2017.02.013
9. H. Nan, X. Hu and H. Tian, *Mater. Sci. Semicond. Process.*, **94**, 35 (2019); https://doi.org/10.1016/j.mssp.2019.01.033
10. Y. Duan, P. Ohodnicki, B. Chorpening and G. Hackett, *J. Solid State Chem.*, **256**, 239 (2017); https://doi.org/10.1016/j.jssc.2017.09.016
11. M. Choi, A.B. Posadas, C.A. Rodriguez, A. O'Hara, H. Seinige, A.J. Kellock, M.M. Frank, M. Tsoi, S. Zollner, V. Narayanan and A.A. Demkov, *J. Appl. Phys.*, **116**, 043705 (2014); https://doi.org/10.1063/1.4891225
12. H. Muta, K. Kurosaki and S. Yamanaka, *J. Alloys Compd.*, **392**, 306 (2005); https://doi.org/10.1016/j.jallcom.2004.09.005
13. U. Sulaeman, S. Yin and T. Sato, *Adv. Nanopart.*, **2**, 6 (2013); https://doi.org/10.4236/anp.2013.21002
14. H. Peng, J. Liang, R. Zhao, F. Wang, G. Wei, J. Zhou, G. Ma and Z. Lei, *Electrochim. Acta*, **300**, 290 (2019); https://doi.org/10.1016/j.electacta.2019.01.135
15. W. Wang, B. Lin, H. Zhang, Y. Sun, X. Zhang and H. Yang, *J. Phys. Chem. Solids*, **124**, 144 (2019); https://doi.org/10.1016/j.jpcs.2018.09.011
16. M. Miyauchi, M. Takashio and H. Tobimatsu, *Langmuir*, **20**, 232 (2004); https://doi.org/10.1021/la0353125
17. J. Wang, S. Yin, M. Komatsu and T. Sato, *J. Eur. Ceram. Soc.*, **25**, 3207 (2005); https://doi.org/10.1016/j.jeurceramsoc.2004.07.027
18. Y. Haruyama, Y. Aiura, H. Bando, H. Suzuki and Y. Nishihara, *Physica B*, **237-238**, 380 (1997); https://doi.org/10.1016/S0921-4526(97)00238-X
19. H. Zhao, J. Xia, D. Yin, M. Luo, C. Yan and Y. Du, *Coord. Chem. Rev.*, **390**, 32 (2019); https://doi.org/10.1016/j.ccr.2019.03.011
20. C. Pratapkumar, S.C. Prashantha, H. Nagabhushana, M.R. Anilkumar, C.R. Ravikumar, H.P. Nagaswarupa and D.M. Jnaneshwara, *J. Alloys Compd.*, **728**, 1124 (2017); https://doi.org/10.1016/j.jallcom.2017.09.058
21. M. Qin, F. Gao, G. Dong, J. Xu, M. Fu, Y. Wang, M. Reece and H. Yan, *J. Alloys Compd.*, **762**, 80 (2018); https://doi.org/10.1016/j.jallcom.2018.05.202
22. B. Avinash, C.R. Ravikumar, M.R.A. Kumar, H.P. Nagaswarupa, M.S. Santosh, A.S. Bhatt and D. Kuznetsov, *J. Phys. Chem. Solids*, **134**, 193 (2019); https://doi.org/10.1016/j.jpcs.2019.06.012

23. M.R.A. Kumar, C.R. Ravikumar, H.P. Nagaswarupa, B. Purshotam, B.A. Gonfa, H.C.A. Murthy, F.K. Sabir and S. Tadesse, *J. Environ. Chem. Eng.*, **7**, 103468 (2019); https://doi.org/10.1016/j.jece.2019.103468
24. K.M. Girish, S.C. Prashantha, H. Nagabhushana, C.R. Ravikumar, H.P. Nagaswarupa, Ramachandra Naik, H.B. Premakumar, B. Umesh, *J. Sci.: Adv. Mater. Devices*, **3**, 151 (2018); https://doi.org/10.1016/j.jsamd.2018.02.001
25. M.R.A. Kumar, H.P. Nagaswarupa, C.R. Ravikumar, S.C. Prashantha, H. Nagabhushana and A.S. Bhatt, *J. Phys. Chem. Solids*, **127**, 127 (2019); https://doi.org/10.1016/j.jpcs.2018.12.012
26. C.R. Ravikumar, M.S. Santosh, H.P. Nagaswarupa, S.C. Prashantha, S. Yallappa and M.R. Anil Kumar, *Mater. Res. Express*, **4**, 065503 (2017); https://doi.org/10.1088/2053-1591/aa73a5
27. Y. Li, S. Li, D. Zhou, A. Wang, P. Zhang, C. Li and J. Feng, *J. Solid State Electrochem.*, **18**, 2521 (2014); https://doi.org/10.1007/s10008-014-2498-8
28. C.R. Ravi Kumar, P. Kotteeswaran, M.S. Santosh, V. Bheemaraju, B. Shruthi, M.S. Shivakumara and H.P. Nagaswarupa, *Asian J. Chem.*, **28**, 221 (2016); https://doi.org/10.14233/ajchem.2016.19355
29. C.R. Ravi Kumar, P. Kotteeswaran, V.B. Raju, B. Shruthi, M.S. Santosh, H.P. Nagaswarupa, M.S. Shivkumar and A. Murugan, *Asian J. Chem.*, **28**, 575 (2016); https://doi.org/10.14233/ajchem.2016.19416
30. H.R. Raveesha, S. Nayana, D.R. Vasudha, J.P. Shabaaz Begum, S. Pratibha, C.R. Ravikumar and N. Dhananjay, *J. Science: Adv. Mater. Devices*, **4**, 57 (2019); https://doi.org/10.1016/j.jsamd.2019.01.003
31. X. Shen and K. Sasaki, *Int. J. Hydrogen Energy*, **41**, 17044 (2016); https://doi.org/10.1016/j.ijhydene.2016.08.024
32. F. Tao, Y. Shen, Y. Liang and H. Li, *J. Solid State Electrochem.*, **11**, 853 (2007); https://doi.org/10.1007/s10008-006-0232-x
33. R. Ranjitha, A.S. Bhatt, C.R. Ravikumar, M.S. Santosh, B.K. Jayanna, H.P. Nagaswarupa, K. Sakai and H. Madhyastha, *Mater. Res. Express*, **6**, 1150d6 (2019); https://doi.org/10.1088/2053-1591/ab5033
34. F. Gobal and M. Faraji, *Ionics*, **21**, 525 (2015); https://doi.org/10.1007/s11581-014-1177-1